RSC Advances

PAPER

View Article Online
View Journal | View Issue

Cite this: RSC Adv., 2015, 5, 74994

Electroactive graphene-multi-walled carbon nanotube hybrid supported impedimetric immunosensor for the detection of human cardiac troponin-I

Shobhita Singal,[ab] Avanish K. Srivastava,[a] Sanjay Dhakate,[a] Ashok M. Biradar[a] and Rajesh*[ab]

We report an electroactive 3-dimensional graphene-multi walled carbon nanotube (G-MWCNT) hybrid prepared using a one step chemical vapor deposition (CVD) method with acetylene as a precursor source, transferred over a glassy carbon electrode (GCE) as a biomolecular immobilization material, for the construction of a bioelectrode. G-MWCNT/GCE was covalently immobilized with human cardiac troponin antibody (anti-cTnI) through a molecular bi-linker, 1-pyrene butyric acid *N*-hydroxysuccinimide ester (PyBuNHS), and characterized by spectroscopy and electrochemical techniques. The bio-analytical performance of the electrode was investigated using electrochemical impedance spectroscopy (EIS) by fitting the impedance response of the electrode with an optimal fitted equivalent circuit model for the quantitative detection of human cardiac troponin (cTnI) in human serum. A low value of exponent '*n*' ($n = 0.44$) observed in a constant phase element of the impedance of the G-MWCNT/GCE hybrid electrode indicated a heterogeneous microstructure surface that exhibited diffusive characteristics but showed dominant charge transfer characteristics (R_{et}) with $n = 0.88$ upon biomolecular immobilization and subsequent immunoreaction with target cTnI in the low frequency region of <1 Hz, showing a good biocompatibility. The bioelectrode exhibited a linear impedance response to cTnI in a wide range of 0.001–10 ng mL^{-1} in human serum with a low detection limit of 0.94 pg mL^{-1} and a sensitivity of 63.5 Ω cm^2 per decade.

Received 3rd August 2015
Accepted 17th August 2015

DOI: 10.1039/c5ra15449a

www.rsc.org/advances

1. Introduction

For the last two decades, graphene, a two-dimensional architecture of sp^2 bonded carbon atoms, has gained enormous scientific attention due to its remarkable physicochemical properties and potential applications.[1] Graphene has outstanding properties, including a large surface area, high heterogeneous electron transfer rates, excellent thermal and electrical conductivity, high intrinsic mobility, high Young's modulus, and enhanced electrochemical behavior. These properties make it a leading potential material for actuators, solar cells, fuel cells, batteries, supercapacitors and electrochemical biosensors.[2–6] Owing to its excellent electrical properties and huge accessible surface area, graphene and its surface modified derivatives have been reported as advanced transducer candidates for electrochemical biosensing applications.[7] However, for practical applications, monolayer graphene is quite difficult to handle, due to its ultra-thin structure and flexibility, which causes it to easily curl, fold, and corrugate.[8–11] This significantly decreases the conductivity and accessible surface area of the monolayer graphene. On the other hand, carbon nanotubes, cylindrical graphene sheets with nanometer diameter, have high mechanical strength, good electrical conductivity, chemical stability and high surface area;[12] however, the electrical conductivity of CNTs is affected by the non-uniform contact and discontinuities between all the CNTs in heterogeneous structures,[13] thereby limiting their applications in sensors.[14–16] In this regard, the combination of one-dimensional carbon nanotubes and two-dimensional graphene into a three dimensional hybrid (G-CNT) is considered to be one of the most effective strategies to fabricate advanced carbon nanostructures[17] with outstanding properties that are superior to either CNTs or graphene alone.[18] The high quality, low cost and large scale production of G-CNT hybrids with well controlled structures is a prerequisite for their bulk applications. Numerous methods have been explored for the preparation of G-CNT hybrids, among which the separate growth of two nanostructures, followed by their mechanical assembly into a single device, is the most explored method to date.[19] Post-synthesis methods, including hydrothermal processes,[20]

[a]CSIR-National Physical Laboratory, Dr K.S. Krishnan Road, New Delhi-110012, India. E-mail: rajesh_csir@yahoo.com
[b]Academy of Scientific & Innovative Research (AcSIR), New Delhi, India

electrophoretic deposition,[21] layer-by-layer assembly,[22] and liquid phase reaction routes,[23] have also been found to be effective for the fabrication of G-CNT hybrids. However, these post synthesis methods are ineffective in creating covalent C–C bonding between graphene and the CNTs in the hybrids; moreover, they are also quite tedious, which significantly limits their performance in a number of applications. In comparison, the direct growth of G-CNT hybrids through chemical vapor deposition (CVD) is more attractive due to the possibility to provide covalent C–C bonding between graphene and CNTs, a lower defect density compared to multi-step routes, and ease of scaling. Recent efforts at fabricating such hybrid architectures have involved growing CNTs on the surface of graphene oxide (GO) or reduced GO coated with catalyst nanoparticles.[24] However, the CNTs grown in such G-CNT hybrids suffer from a poor degree of graphitization due to the high dissolution of catalyst NP in GO and reduced GO.[25] Therefore, it would be quite advantageous to construct a 3D G-CNT hybrid nanostructure in a one-step CVD process, involving the simultaneous growth of graphene and CNT on an iron nanoparticle (Fe NP) deposited copper foil.

Cardiac troponin-T and I (cTnT and cTnI) are highly sensitive and specific biomarkers[26] for myocardial injury and have been accepted by the World Health Organization (WHO) for the diagnosis of acute myocardial infarction (AMI). cTnI has high cardio-specificity and is virtually absent in skeletal muscle tissue, whereas cTnT is expressed in skeletal muscle to a smaller extent. cTnI, with a molecular weight of 29 kDa,[27] is a part of a troponin complex that is present in cardiac muscles. During myocardial damage, the troponin complex is broken up and cTnI is released into the bloodstream. The cut-off concentration of cTnI in the blood is 0.01–0.1 ng ml^{-1}. Upon acute myocardial infarction, the cTnI concentration in serum dramatically increases within the range of 10–24 h, and its elevation in the blood persists up to 10–14 days.[28] When the cTnI concentration reaches 0.2–1.4 ng mL^{-1}, minor myocardial injury can be concluded, whereas significant myocardial necrotic damage should be considered when cTnI levels are elevated over 1.5 ng mL^{-1}.[29] The cardio-specificity of cTnI, along with its long persistence in the blood, makes it the "gold standard" biomarker that provides an extended diagnostic window for the detection of AMI. Thus, reliable and early quantification of cTnI concentration is highly desirable to improve the outcome of cardiovascular disease. Various traditional techniques, such as chemiluminescent immunoassays, enzyme-linked immunosorbent assays (ELISA) and radio immunoassays, are used for the quantification of cTnI. However, these techniques involve complicated multistage processes that are tedious and time-consuming. Electrochemical impedance spectroscopy (EIS) has received considerable attention in recent years due to its sensitive, rapid and non-destructive nature. The quantification of cTnI in an aqueous solution or serum is obtained using its antigen–antibody (Ag–Ab) coupling mechanism, wherein these couples of cTnI disturb the electrode layer by ion diffusion, causing changes in the electrical impedance.

In the present study, we report the fabrication of highly conductive, large area three dimensional G-MWCNT hybrid film on a glassy carbon electrode (GCE) as an impedimetric immunosensor for highly sensitive detection of the human cardiac troponin I (cTnI) biomarker. The G-MWCNT hybrid film was synthesized by a simple single step atmospheric CVD process on a Fe NP decorated copper foil and transferred onto a glassy carbon electrode (GCE). The G-MWCNT/GCE electrode was biofunctionalized with a bio-receptor, anti-cTnI, through a bi-linker, 1-pyrenebutyric acid *N*-hydroxysuccinimide ester (PyBuNHS), using a carbodiimide coupling reaction to an anti-cTnI-PyBuNHS/EG-MWCNT/GCE bioelectrode. The microstructural and electrochemical characteristics of the hybrid film were systematically characterized by various spectroscopy techniques such as scanning electron microscopy (SEM), transmission electron microscopy (TEM), Raman spectroscopy and electrochemical techniques. The bioanalytical performance of the bioelectrode was investigated for the quantitative detection of cTnI in human serum by electrochemical impedance spectroscopy (EIS).

2. Experimental

2.1 Reagents

Anti-cardiac troponin I (anti-cTnI; Cat 4T21 MAb 19C7) and human cardiac troponin I (cTnI; Cat 8T53) were obtained from Hytest (Turku, Finland). Mouse immunoglobulin-G (IgG) (Cat IGP3) was obtained from GENEI, Bangalore, India. 1-Pyrenebutyric acid *N*-hydroxysuccinimide ester (PyBuNHS), *N*-(3-dimethylaminopropyl)-*N*′-ethyl carbodiimide hydrochloride (EDC), and *N*-hydroxy succinimide 98% (NHS) were obtained from Sigma-Aldrich Corp. All other chemicals were of analytical grade and used without further purification.

2.2 Apparatus

TEM images were obtained on a high resolution TM model Technai G2F30 Stwin. SEM images were obtained on an FE-SEM model SUPRA40 VP, Germany. Raman spectra of graphene were obtained on a Renishaw Raman Spectrometer, Germany, with a laser excitation source at 514 nm. Cyclic voltammetry (CV) and EIS measurements were performed on a PGSTAT302N, AUTOLAB instrument from Eco Chemie, the Netherlands. The EIS parameters were obtained by circuit fitting the EIS experimental data using GPES (General purpose electrochemical system version 4.9, Eco Chemie) software. All electrochemical measurements were carried out in a conventional three-electrode cell configuration consisting of the proposed bioelectrode as the working electrode, Ag/AgCl as the reference electrode and platinum wire as the counter electrode.

2.3 Synthesis of G-MWCNT

The G-MWCNT hybrid films were grown by atmospheric CVD on a copper foil ($\sim$2.54 cm^2) decorated with 1 nm thick Fe NP using an e-beam evaporator. The Fe NP and copper foil acted as catalysts for MWCNT and graphene growth, respectively. The Fe NP decorated copper foil was positioned in the interior of a fused silica tube (inside diameter 5 cm, length 100 cm) maintained in a heating furnace, and the temperature was elevated to

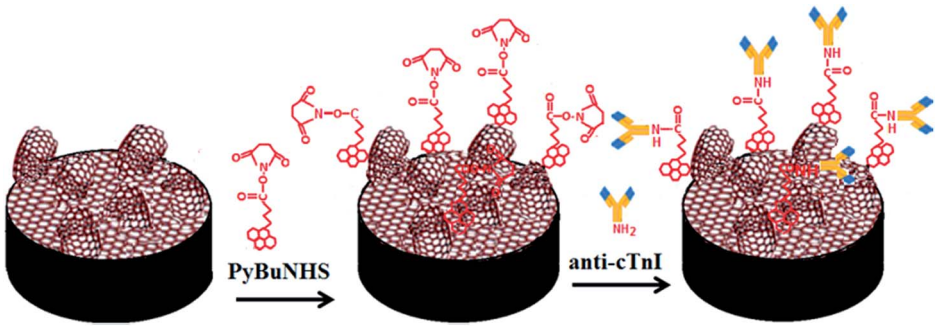

Fig. 1 Schematic of the stepwise fabrication of the bioelectrode.

750 °C under a 200 sccm (standard cubic centimetre per min)/100 sccm continuous flow of Ar/H_2. Once the temperature of the furnace was stabilized to 750 °C, a 10 sccm flow of C_2H_2 was introduced for 20 min, followed by cooling of the furnace to room temperature under Ar/H_2 atmosphere. Graphene film grown on the back side of the Cu foil was burnt off using reactive ion etching (RIE), followed by etching of the Cu foil in 1 M aqueous $FeCl_3$ solution to obtain the G-MWCNT hybrid film; the film was washed repeatedly with deionized water and aqueous HCl (5%) to remove metal impurities, as reported earlier.[30]

2.4 Preparation of anti-cTnI–PyBu/EG-MWCNT/GCE

GCE was mechanically polished with 1, 0.3 and 0.05 μm alumina powder, followed by sonication in distilled water and drying under vacuum. The G-MWCNT hybrid film was transferred onto the GCE surface (3 mm diameter) by careful scooping and was dried at 50 °C for 1 h to obtain the G-MWCNT/GCE electrode.

G-MWCNT mounted on GCE was pretreated by anodization at a potential of 1.7 V *vs.* Ag/AgCl for 500 s in pH 7.4 PBS, followed by cathodization at −0.6 V for 60 s to obtain electroactive G-MWCNT (EG-MWCNT/GCE). This treatment of G-MWCNT introduced defects on the edge planes of the graphene and the ends of the carbon nanotubes with the generation of carbonyl groups during oxidation that were subsequently reduced to C–OH, leading to enhanced electroactive behavior of the G-MWCNT hybrid, as reported earlier for GCE.[31] The EG-MWCNT was treated with a molecular bi-linker, PyBuNHS, for the covalent attachment of anti-cTnI using a carbodiimide coupling reaction. 10 μL of 2 mM PyBuNHS in DMF was drop casted on EG-MWCNT/GCE and incubated for 40 min at room temperature, followed by extensive washing with DMF, and then dried under N_2 gas flow to obtain the PyBuNHS functionalized EG-MWCNT/GCE through π–π stacking. The PyBuNHS/EG-MWCNT/GCE was biofunctionalized with a bioreceptor, anti-cTnI, by incubating it with 10 μL PBS containing 100 μg mL^{-1} anti-cTnI at 4 °C for 2 h, followed by washing with PBS and drying under N_2 gas flow. The abovementioned biofunctionalized electrode was then incubated with 0.1% (w/v) bovine serum albumin (BSA) to block the non-specific binding sites on the electrode surface, followed by washing with PBS to remove any physically adsorbed antibodies and drying under N_2 flow to obtain the desired anti-cTnI–PyBu/EG-MWCNT/GCE bioelectrode. The stepwise fabrication of the bioelectrode is schematically represented in Fig. 1. For a comparative bioanalytical performance study, a biofunctionalized pristine graphene bioelectrode, anti-cTnI–PyBuNHS/EG/GCE, was also prepared using a bare copper foil by following the same procedure, as described above and stored at 4 °C.

3. Results and discussion

3.1 Surface morphological characterization of G-MWCNT hybrid

Morphological characterization of the G-MWCNT hybrid was carried out by employing SEM, TEM, and Raman spectroscopy. The CVD grown G-MWCNT hybrid film was transferred over a SiO_2/Si wafer to acquire the SEM images. As shown in the SEM image (Fig. 2a), the one-step G-MWCNT synthesis method produced highly dense multi-walled CNTs with an average tube diameter of 60 nm growing uniformly over the entire large-area graphene surface. Raman spectroscopy was instrumental in characterizing the structure and crystalline quality of the G-MWCNT hybrid. Raman spectra acquired of the hybrid on copper foil (Fig. 2b) showed well defined D, G, 2D, and D + G characteristic peaks at 1348 cm^{-1}, 1590 cm^{-1}, 2698 cm^{-1}, and 2941 cm^{-1}, respectively. The two dominant peaks (D and G) showed strong intensities and sharp profiles, and their intensity ratios (I_D/I_G) were used to estimate the defect level in the G-MWCNT hybrid. The I_D/I_G intensity ratio of 1.71 corresponds to a high value of defects with more sp^3 disorder than sp^2 order in the G-MWCNT hybrid. The disorder-induced D band is supposed to originate from crystal defects such as grain boundaries, whereas the G band originates from the in-plane vibration mode E_{2g}.[32] The third common peak, generally referred to as the 2D peak, occurs due to the second order vibrations of the C–C bond and provides information about the two dimensional graphitic stacking of the carbon materials. The I_{2D}/I_G ratio of 0.47 indicates that graphene is mostly tri-layer (few layer) in thickness in the G-MWCNT hybrid.

High resolution transmission electron microscopy (HRTEM, model: Tecnai G2F30 STWIN) was employed to investigate the pristine graphene and the G-MWCNT hybrid. It is important to elucidate that a large area of graphene nanosheet was revealed

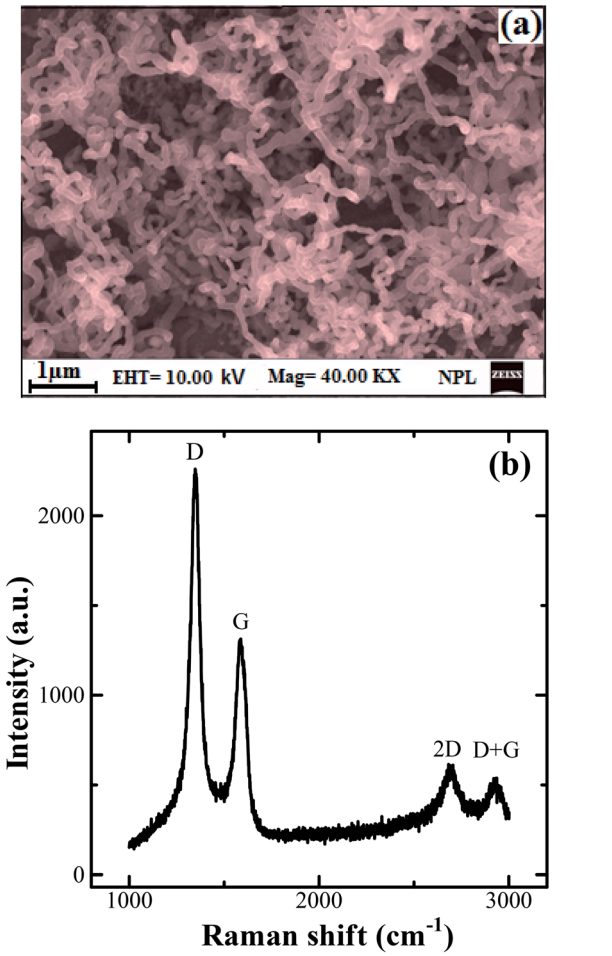

Fig. 2 (a) SEM micrograph of the G-CNT hybrid film on a Si substrate; (b) Raman spectra of the G-MWCNT hybrid on Cu foil.

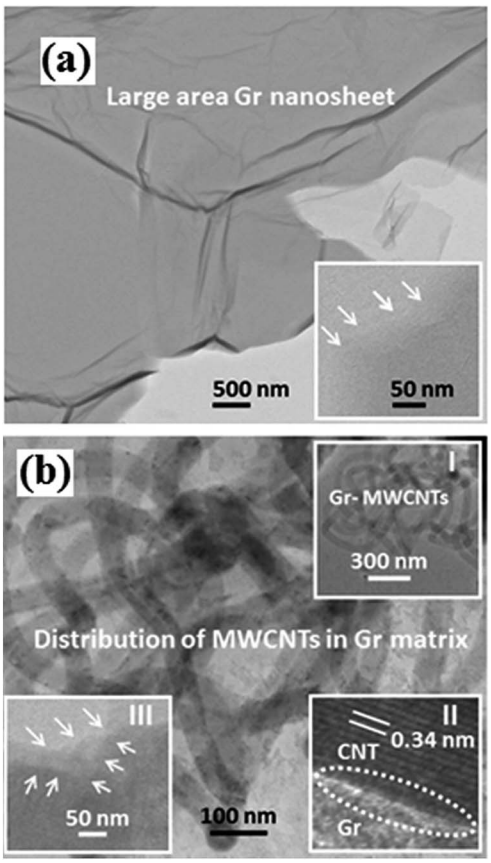

Fig. 3 HRTEM micrographs showing (a) large area graphene nanosheets and (b) the distribution of MWCNTs in the matrix of the graphene sheet. Inset in (a): high magnification of the edges of graphene sheet; inset I in (b): dense distribution of the MWCNTs in graphene; inset II in (b): interface between MWCNT and the graphene sheet; and inset III in (b): edges of the multilayered graphene nanosheet.

throughout the specimen in the case of pristine graphene (Fig. 3a). Wrinkles occurring at instances in the graphene sheet may be attributed to mechanical strain that occurred during the transfer of the material onto the TEM grid.

At high magnification, it was further delineated that at the edges of the films (marked with a set of white arrows in the inset of Fig. 3a) we did not see any contrast and therefore, these sheets are seemingly single instead of multifold. In the composite sample, G-MWCNT hybrid, a high density of MWCNTs is observed in the matrix of the graphene sheet (inset I in Fig. 3b). The carbon nanotubes are spread throughout in the matrix of the graphene with diameters ranging between 50 and 70 nm (Fig. 3b). We further examined the compatibility between the graphene sheet and CNT. As an illustrative example, the atomic scale image of the interface between the graphene and a nanotube (encircled with a white dotted line in the inset II of Fig. 3b) depicts a clean image at the apex of the interface without any microscopic imperfections. Moreover, the interlayer separation between the consecutive walls of the nanotube was measured approximately as 0.34 nm (inset II in Fig. 3b). In this G-MWCNT hybrid sample, effort was made to distinguish the edges of the graphene nanosheets by carrying out focusing/defocusing experiments during the microscopy. The thickness of these sheets varied approximately between 2 and 2.5 nm. It was observed that in general, at least two to three layers of graphene are obvious in these nanosheets. A region revealing multilayered graphene has been demarked with a set of white arrows in inset III of Fig. 3b.

3.2 Electrochemical characterization of anti-cTnI–PyBu/EG-MWCNT/GCE

Cyclic voltammetry (CV) is an efficient and widely used electroanalytical technique, which provides useful information regarding the surface status of electrodes. Theoretically, the alteration in the peak current and peak potential positions in CV at distinct electrode surfaces are linked to the electron transfer resistance. Each step of the surface modification of GCE and antibody immobilization was monitored by CV measurements performed in a PBS solution (pH 7.4; 0.1 M KCl) containing a mixture of 2 mM $K_3[Fe(CN)_6]$ and 2 mM $K_4[Fe(CN)_6]$ as a redox probe at a scan rate of 50 mV s^{-1}. Fig. 4 shows the CV response of the modified electrode before and after the immobilization of a bioreceptor, anti-cTnI. The GCE shows a couple of reversible redox peaks with a peak-to-peak separation between the

oxidation and reduction potentials (ΔE_p) of 140 mV, indicating that the GCE has a clean and active surface. The GCE after modification with CVD grown G-MWCNT hybrid film showed an enhanced redox peak current. This outstanding electron transfer ability of the G-MWCNT hybrid film modified GCE electrode surface is attributed to the large active surface area and high conductivity of the G-MWCNT hybrid. It can be noted that the electrochemical behavior of the G-MWCNT hybrid is strongly dependent on the density of defects, edges, and porous features. There has been evidence in the literature that anodized CNT, which contains oxygen related defects, is a superior platform for protein interaction.[31] Thus, we simultaneously anodized and cathodized the G-MWCNT surface to create edge plane defects and porous features to facilitate fast electron transfer kinetics, leading to a smaller interpeak distance of 59 mV and an enhanced redox peak current, as is evident in the CV (Fig. 4). A comparative CV response of the anodized electroactive 3D EG-MWCNT/GCE hybrid and 2D pristine graphene (EG/GCE) electrodes is shown in the inset of Fig. 4. The electroactive surface area of both the 3D and 2D structures was estimated using the Randles–Sevcik[33] equation (eqn (1)):

$$I_p = 2.69 \times 10^5 A D^{1/2} n^{3/2} \nu^{1/2} C \quad (1)$$

where n is the number of electrons participating in the redox reaction (1 in this case), A is the electroactive surface area (cm^2), $D = 6.70 \times 10^{-6}$ cm^2 s^{-1}, which is the diffusion coefficient of $[Fe(CN)_6]^{3-}$ in the solution, C corresponds to the concentration of the redox probe ($K_3[Fe(CN)_6]$, 0.002 M), and ν is the scan rate of the potential perturbation (mV s^{-1}). The electroactive surface area of the 3D EG-MWCNT hybrid and 2D EG electrodes were found to be 0.159 and 0.084 mm^2, respectively, showing that the surface area for the 3D hybrid was ~2.1 times larger than that of EG. A decrease in the redox peak current with an increased ΔE_p of 76 mV was observed upon treatment of EG-MWCNT/GCE with PyBuNHS due to the hydrophobic character of PyBuNHS as well as to the formation of a physical barrier that decreases the flux of the probe to the electrode surface, showing sluggish heterogeneous electron transfer kinetics; this confirms the formation of modified PyBuNHS/EG-MWCNT/GCE. Subsequent decreases in the redox peak currents were observed after the biomolecular immobilization of PyBuNHS/EG-MWCNT/GCE with a bioreceptor, anti-cTnI, and its surface passivation with a blocking protein, BSA; this may be attributed to the perturbation of the electron penetration by the insulating layer of the protein backbone molecules at the modified electrode surface.

The electrochemical properties of both the 3D and 2D structures after protein antibody immobilization were further investigated by EIS measurements in the applied frequency region of 0.01 Hz to 10 kHz. The equivalent circuit, which is often used to model interfacial phenomena, is called Randle's circuit and includes the following four elements: (i) the ohmic resistance of the electrolyte solution, R_s; (ii) the Warburg impedance, Z_w, resulting from the diffusion of the ions from the bulk electrolyte to the electrode interface; (iii) the interfacial double layer capacitance, C_{dl}, relating to the surface characteristics of the electrode and (iv) the charge transfer resistance, R_{et}.

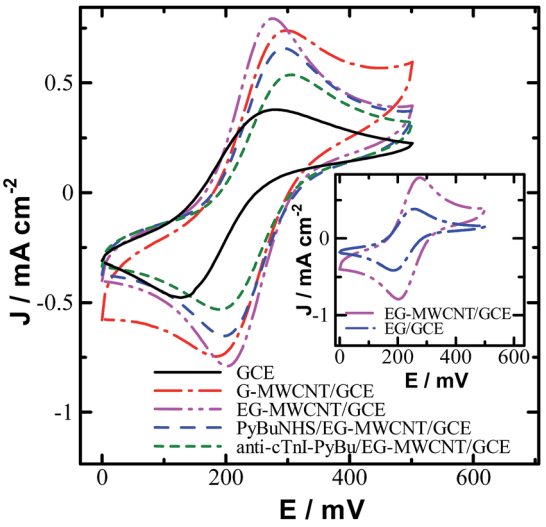

Fig. 4 CV of the bioelectrode at different stages of fabrication in PBS (0.1 M KCl; pH 7.4) containing 2 mM $[Fe(CN)_6]^{3-/4-}$; scan rate 50 mV s^{-1}; 3rd CV scan is shown. Inset: CV of EG/GCE and EG-MWCNT/GCE.

The latter three circuit parameters, C_{dl}, R_{et} and Z_w, are dependent on the surface microstructural features and are affected by changes in the interfacial properties of the electrode. The inhomogeneous surface morphology of the 3D EG-MWCNT/GCE causes C_{dl} to be replaced by a constant phase element (CPE) to take into account the topological imperfections of the electrode surface. The impedance of a CPE is depicted by eqn (2):

$$Z_Q = 1/j\omega^n Y_{o,} \quad (2)$$

where Y_o is a proportionality constant, ω is the angular frequency ($\omega = 2\Pi f$ in Hz), j is the imaginary number ($j = \sqrt{-1}$) and n ($-1 \leq n \leq 1$) is the frequency power that controls the extent of deviation from the Randle's model and is attributed to the heterogeneity of the electrode surface. CPE can represent capacitance ($C = Y_o$) when $n = 1$; resistance ($R = 1/Y_o$) when $n = 0$; inductance ($L = 1/Y_o$) when $n = -1$ or Warburg impedance when $n = 0.5$. In our case, the value of n for distinct modified electrodes is <1, indicating a pseudo interfacial double layer capacitance at the electrode/electrolyte interface. The chi-squared function (χ^2) of the best fit equivalent circuit to the Nyquist and Bode plots is the measure of the standard deviation between the original data and the calculated spectrum; this was found to be 0.016 for the bioelectrode, and the EIS parameters are given in Table 1. A negligible change in the value of R_s was observed during electrode modification and therefore has been ignored in the discussion. The typical impedance spectrum is represented as a Nyquist plot, and consists two parts: a semi-circle part at a higher frequency range and a straight line part at a lower frequency range, corresponding to the electron transfer-limit process and diffusion-limit process, respectively. The charge transfer resistance (R_{et}) value is often directly determined by measuring the diameter of the semicircle portion. The impedance spectra obtained at different stages of bioelectrode fabrication are shown in Fig. 5.

As seen, after the modification of GCE with G-MWCNT, the value of R_{et} decreased from 74.2 Ω cm^2 to about 57.7 Ω cm^2, indicating an enhanced electron transfer rate ($k^0 = 0.75 \times 10^{-4}$ m s^{-1}) because of the highly electroactive and large surface area offered by the G-MWCNT hybrid film. After the electrochemical treatment of the G-MWCNT hybrid film, the semicircle in the high frequency region almost disappeared, suggesting that the electrode reaction was only controlled by a diffusion limited process. Since an n value of 1 corresponds to a smooth defect free surface and $0 < n < 1$ reflects a rough surface, the significantly low values of $n = 0.44$ and $Z_w = 6.94 \times 10^{-5}$ were obtained for EG-MWCNT/GCE, further indicated an inhomogeneous microstructural electrode surface. The low R_{et} (0.26 Ω cm^2) with a comparatively high Y_o (0.23 mF cm^{-2}) value for the EG-MWCNT hybrid film may be associated with edge plane defects and oxygenated groups on the surface of the EG-MWCNT, which contributed to the increased capacitive charging current.

Since the amount of protein immobilization on the electrode surface depends upon its surface area, the protein amount was calculated and compared on both the 3D and 2D structures (inset of Fig. 5a) using eqn (3) as described earlier:[34]

$$\Gamma = 4RTC/F^2A \quad (3)$$

where A is the electroactive surface area of the electrode, F is the Faraday constant, R is the gas constant, T is the temperature, and C is the capacitance of the adsorbed layer. The amounts of protein adsorbed (Γ) on the 3D EG-MWCNT and 2D EG electrodes were found to be 26.8×10^{-8} mol cm^{-2} and 17.3×10^{-8} mol cm^{-2}, respectively, revealing a comparatively 1.5 fold higher surface protein concentration on the 3D hybrid than on the 2D graphene. This high surface protein concentration on the 3D hybrid may be attributed to its large active surface area as described above during the discussion of the CV measurements. This unique feature of the 3D geometry of the hybrid with a high surface protein concentration has been further investigated as a highly sensitive material for the electrochemical detection of cTnI in human serum.

3.3 Electrochemical impedance response of the hybrid bioelectrode to cTnI

The impedimetric response of the bioelectrode was tested towards the protein antigen, cTnI, spiked in normal human serum. Before EIS measurements, the bioelectrode was incubated with 10 μL individually spiked human serum samples of different cTnI concentrations for 10 minutes, followed by washing with PBS and drying under N_2 gas flow, at room temperature. An incubation time of 10 min was optimized based on the observation of not obtaining any significant change in the impedance of the immunoreaction beyond this time period. The Nyquist plot of the impedance response of the bioelectrode with different concentrations of cTnI spiked human serum is shown in Fig. 6a, wherein the response with non-spiked human serum was taken as a control sample response. The diameter of the semicircle in the Nyquist plot increased gradually upon incubation of the bioelectrode with increasing concentrations of the cTnI spiked human serum due to the antigen–antibody interaction upon immunoreaction, which acts as a kinetic barrier to interfacial electron transfer at the electrode surface, leading to increased electron transfer resistance, R_{et}. Since the change in the value of R_{et} is much more pronounced in comparison to other impedance components (Table 2), it was taken as a suitable signal for sensing the interfacial properties of the bioelectrode.

A continuous decrease in the value of Y_o on immunoreaction with increasing cTnI concentration indicated a decrease in the capacitive behavior of the bioelectrode due to the increasing

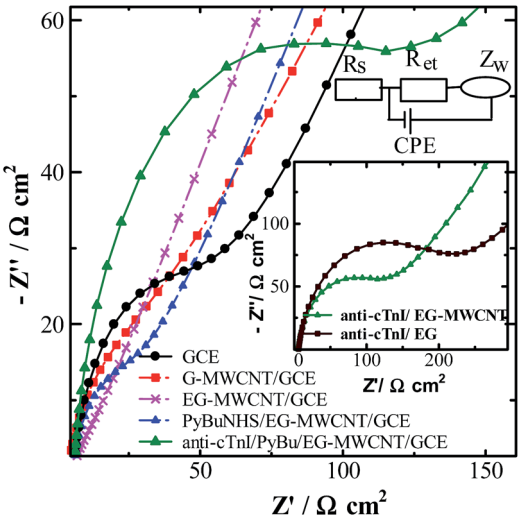

Fig. 5 Nyquist plot obtained at different stages of the bioelectrode fabrication in PBS (0.1 M KCl; pH 7.4) containing 2 mM $[Fe(CN)_6]^{3-/4-}$.

Table 1 CV and EIS characteristic parameters at various stages of electrode surface modifications ΔE_p = redox potential; R_{et} = charge transfer resistance; CPE = constant phase element; k^0 = apparent rate constant; Z_w = Warburg impedance

			CPE				
Type of electrode	ΔE_p (mV)	R_{et} (Ω cm^2)	Y_0 (mF cm^{-2})	n	k^0 (m s^{-1})	Z_w (Ω cm^2)	χ^2 ($\times 10^{-2}$)
Bare GCE	140	74.2	0.09	0.83	3.6×10^{-4}	2.82×10^{-5}	1.35
G-MWCNT/GCE	123	57.7	0.19	0.68	0.75×10^{-4}	3.26×10^{-5}	1.43
EG-MWCNT/GCE	59	0.26	0.23	0.44	10.4×10^{-2}	6.94×10^{-5}	7.84
PyBuNHS/EG-MWCNT/GCE	76	23.3	0.03	0.88	11.6×10^{-4}	5.62×10^{-5}	2.99
Anti-cTnI–PyBuNHS/EG-MWCNT/GCE	90	102.5	0.02	0.88	2.64×10^{-4}	4.76×10^{-5}	1.64
Anti-cTnI–pyBuNHS/EG/GCE	126	196.1	0.01	0.85	1.38×10^{-4}	4.15×10^{-5}	1.86

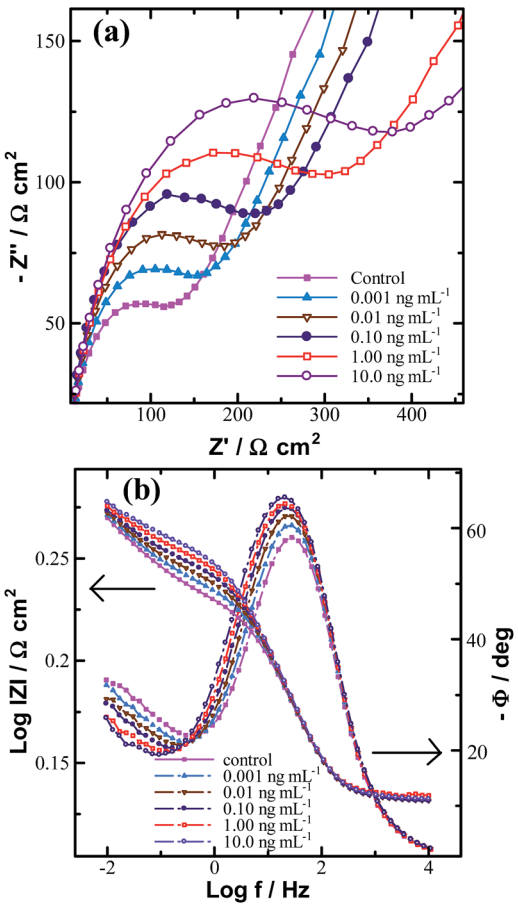

Fig. 6 (a) Nyquist plot of the bioelectrode before and after incubation with different concentrations of cTnI-spiked human serum; (b) corresponding Bode plot.

thickness of the dielectric layer between the electrode and the electrolyte. These results were further elaborated by the corresponding Bode plots (Fig. 6b) in three distinct frequency regions of the high frequency region (>10 Hz), the intermediate frequency region of 1 to 100 Hz and the low frequency region of <1 Hz. At frequency >10 Hz, the impedance was found to be independent of frequency with a nearly zero phase angle (Φ); this corresponds to the solution resistance, R_s. In the intermediate frequency region of 1 to 100 Hz, the slope of the log $|Z|$ *vs.* log f plot was found to be close to −0.7 with the phase shift (Φ) moving from 58° to 65° upon immunoreaction with increasing cTnI concentration at the electrode surface; this indicated a pseudo capacitive behavior of the bioelectrode, as a slope of <−1.0 or a Φ value of ≥90° corresponds to an ideal capacitive behavior. At frequencies <1 Hz, where current/time (I/t) and voltage/time (V/t) are nearly in phases (lowest phase angle), which signifies the frequency independence of the charge transfer characteristics (R_{et}) and the diffusion controlled process (Z_w) of the bioelectrode. The maximum changes in the overall impedance of the bioelectrode on immunoreaction were observed in this low frequency region, R_{et} is the dominant character. It was found that the lowest phase angle (R_{et} dominant character) moved towards a lower frequency on immunoreaction with increasing cTnI concentration, further revealing the good biocompatibility of the bioelectrode.

The equilibrium dissociation constant (K_d) was measured to evaluate the affinity of the antibody to its binding ligand in a bimolecular antibody–antigen interaction. The smaller the K_d value, the greater the affinity of the antibody for its target antigen. The dissociation reaction between the antigen [A] and antibody [Y] for K_d can be represented by eqn (4) & (6):

$$AY \rightarrow A + Y \quad (4)$$

$$K_d = [A][Y]/[AY] \quad (5)$$

Assuming the surface coverage of the antigen–antibody complex is θ, the surface coverage of unbound antibody will be $1 - \theta$, as given in eqn (6):

$$K_d = (1 - \theta/\theta)[A] \quad (6)$$

The value of K_d can be obtained by relating either the charge transfer resistance (R_{et}) or capacitance (C_d) to the surface coverage.[35] Since insignificant changes were observed in the capacitance values (Table 2), we used the R_{et} component for K_d measurement, considering a Langmuir adsorption isotherm and a linear relationship between the surface coverage (θ) and R_{et}^{-1} by eqn (7)–(9).

$$\Delta R_{et}^{-1} = \theta(\Delta R_{et}^{-1})_{max} \quad (7)$$

Table 2 EIS characteristic parameters of the bioelectrode on immunoreaction with different concentrations of cTnI-spiked human serum R_{et} = charge transfer resistance; CPE = constant phase element; Z_w = Warburg impedance; RSD = relative standard deviation

		CPE				
Immunoreaction with [cTnI]	R_{et} (Ω cm²)	Y_0 (mF cm^{-2})	n	Z_w (Ω cm²)	χ^2 (10^{-2})	RSD (%) (n = 3)
Control	102.5	0.029	0.887	4.76×10^{-5}	1.64	—
0.001 ng mL^{-1}	156.2	0.028	0.885	4.73×10^{-5}	1.56	3.22
0.010 ng mL^{-1}	207.6	0.028	0.883	4.74×10^{-5}	1.62	7.06
0.10 ng mL^{-1}	276.2	0.027	0.887	4.73×10^{-5}	1.66	6.43
1.00 ng mL^{-1}	323.3	0.025	0.882	4.68×10^{-5}	3.17	9.00
10.0 ng mL^{-1}	405.4	0.023	0.887	4.65×10^{-5}	2.61	2.82

where

$$\Delta R_{et}^{-1} = [(R_{et}^{-1})_{\theta=0} - R_{et}^{-1}]/(R_{et}^{-1})_{\theta=0} \quad (8)$$

and

$$\Delta\,(R_{et}^{-1})_{max} = [(R_{et}^{-1})_{\theta=0} - (R_{et}^{-1})_{max}]/(R_{et}^{-1})_{\theta=0} \quad (9)$$

The R_{et} change was taken into the Hanes–Woolf form to avoid overloading of the data at low protein concentrations and can be described by eqn (10):

$$[A]/\Delta R_{et}^{-1} = [A]/\Delta\,(R_{et}^{-1})_{max} + K_d/\Delta\,(R_{et}^{-1})_{max} \quad (10)$$

wherein the dissociation constant was calculated by dividing the intercept by the slope obtained from the corresponding plot shown in Fig. 7. K_d was found to be 1.52 ng mL^{-1}, which corresponds to 5.2×10^{-11} M and is quite comparable to earlier reports.[36] This low value of K_d indicated a strong binding affinity of anti-cTnI towards the target cTnI in an antigen–antibody interaction at the electrode surface.

Fig. 8 shows the calibration curve of the bioelectrode, depicting a linear relationship between the change in charge transfer resistance ($\Delta R_{et} = (R_{et})_{after\ immunoreaction} - (R_{et})_{control}$) and the logarithmic concentration of target cTnI over the concentration range from 0.001 to 10 ng mL^{-1} cTnI, which can be represented by eqn (11):

$$\Delta R_{et}(\log[cTnI]) = b \log[cTnI] + 245.37 \quad (11)$$

The bioelectrode shows an R_{et} sensitivity (slope b of the calibration curve) of 63.5 Ω cm^2 per decade of cTnI with a correlation coefficient of 0.99. The points of the calibration curve represent the average of three independent measurements with relative standard deviations from 2.8% to 9%, which are shown in the form of error bars.

The reproducibility of the bioelectrode response was examined by recording the impedance of the three different individual bioelectrodes, prepared at different times, with cTnI concentrations in the range from 0.001 to 10 ng mL^{-1}. The RSD of the resulting impedance response of the bioelectrode did not exceed 9% in any case, exhibiting good reproducibility performance within the acceptable error range. The results demonstrate that ΔR_{et} is linear with the logarithmic value of cTnI concentration over a range of 0.01 to 10 ng mL^{-1} with R_{et} sensitivity of 63.5 Ω cm^2 per decade of cTnI. This R_{et} sensitivity was found to be ~1.5 times higher than the sensitivity (44.3 Ω cm^2 per decade) obtained with a pristine 2D graphene based bioelectrode (EG/GCE); a comparative sensing performance experiment, carried out under identical experimental conditions, demonstrated the advantage of using the high surface 3D G-MWCNT hybrid in a biosensing electrode. The limit of detection (LOD) of the hybrid bioelectrode was found to be 0.94 pg mL^{-1} based on three times the signal-to noise ratio, which is a much lower concentration than the recently reported 0.2 ng mL^{-1} in the case of a similar carbon nanofibre based impedimetric biosensor. The LOD obtained has further been compared with other electrochemical detection techniques given in Table 3, underlining the superiority of the present platform system. The stability of the bioelectrode was also investigated by carrying out repeated EIS measurements with the same dispensed cTnI-spiked human serum sample, and the corresponding R_{et} response was measured. It was found that an almost constant R_{et} response was observed even after more than 5 repeated measurements, indicating the good stability of the bioelectrode in the solution. The specificity of the bioelectrode was examined by evaluating the normalized resistance response ΔR_{et} (%) upon exposure to each 10 ng mL^{-1} concentration of non-specific IgG and another cardiac biomarker, C-reactive protein (CRP) spiked human serum samples, under identical experimental conditions. It was observed that both the IgG and CRP contributed insignificantly to the total response with 10.2% and 7.4%, respectively, with respect to cTnI (inset of Fig. 8), indicating the high selectivity of the bioelectrode towards cTnI.

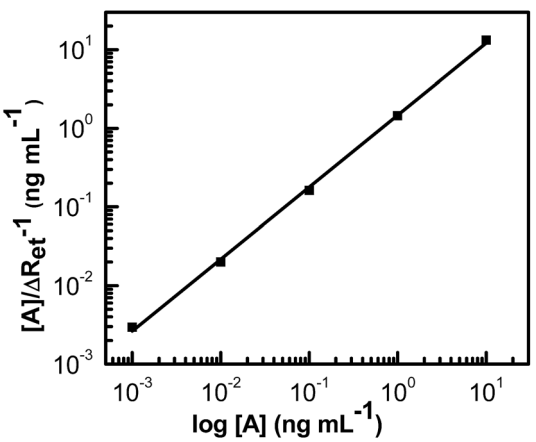

Fig. 7 Hanes–Woolf plot for determining the dissociation constant (K_d) between cTnI and anti-cTnI.

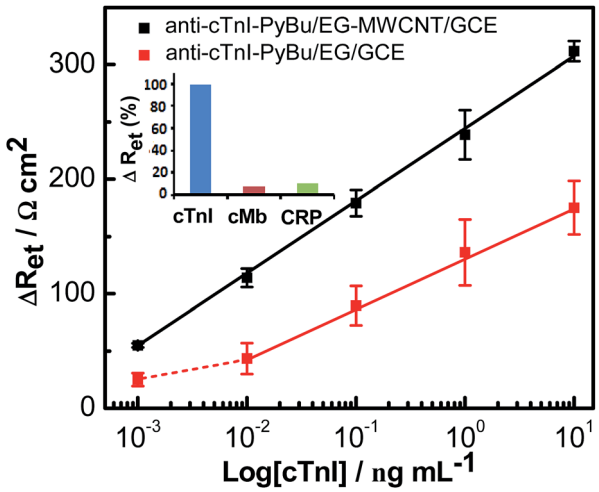

Fig. 8 Concentration dependent calibration curve of the bioelectrode; inset: normalized response ΔR_{et} (%) of the bioelectrode towards non-specific CRP and IgG with respect to cTnI.

Table 3 Comparative analytical performance of the bioelectrode with existing electrochemical systems for cTnI detection

Sensing technique	Transducing matrix	Detection range	Limit of detection	Ref.
Amperometry	PDMS/Au	0.2 ng mL^{-1} to 10.0 μg mL^{-1}	148 pg mL^{-1} (ref. 27)	27
Capacitive	Au/screen printed electrode	0.2 ng mL^{-1} to 12.5 ng mL^{-1}	0.2 ng mL^{-1}	28
Impedimetric	mSAM/Au	2.9 pg mL^{-1} to 2.9 μg mL^{-1}	2.9 pg mL^{-1}	36
Impedimetric	Carbon nanofibre	0.25 ng mL^{-1} to 1.0 ng mL^{-1}	0.2 ng mL^{-1}	37
Stripping voltammetry	Ag/screen printed electrode	0.10 ng mL^{-1} to 32.0 ng mL^{-1}	0.1 ng mL^{-1}	38
Amperometry	Screen printed electrode	0.50 ng mL^{-1} to 50.0 ng mL^{-1}	0.1 ng mL^{-1}	39
Potentiometry	Au/indium-tin-oxide	1.0 ng mL^{-1} to 100.0 ng mL^{-1}	—	40
Impedimetric	G-MWCNT/GCE	1.0 pg mL^{-1} to 10.0 ng mL^{-1}	0.94 pg mL^{-1}	Present work

4. Conclusions

In this study, we demonstrated a G-MWCNT hybrid modified GCE for the biomolecular immobilization of a highly specific human cardiac bioreceptor, anti-cTnI, acting as a platform for the quantitative impedimetric detection of the cardiac protein antigen, cTnI. The microstructural and electrochemical characteristics of the bioelectrode have been extensively characterized by SEM, TEM, Raman spectroscopy and electrochemical techniques. The conjugation of 2D graphene and the percolating network of 1D CNTs results in a quasi-3D conduction network with exceptionally high electroactive features and a large surface area, leading to an enhanced and effective loading of the bioreceptor in the analytically active layer, providing a wide range of cTnI detection from 0.001 to 10 ng mL^{-1} concentration in human serum. The EIS studies of the bioelectrode showed dominant R_{et} characteristics towards target cTnI on immuoreaction in the low frequency region of <1 Hz, indicating a good biocompatible feature. The bioelectrode exhibited a low value of dissociation constant, K_d of 5.2×10^{-11} M, showing strong binding affinity towards the target cTnI with high sensitivity, which is about 1.5 fold higher than that of the electrode fabricated with 2D-pristine graphene; this indicates a strong antigen–antibody interaction at the electrode surface. The bioelectrode showed a low detection limit of 0.94 pg mL^{-1} cTnI, which is much lower than those recently reported in the literature. These results indicate that the abovementioned G-MWCNT hybrid modified electrode may be used to immobilize other enzymes, proteins or DNA for various biological and electrochemical applications.

Acknowledgements

We are grateful to the Director, National Physical Laboratory, New Delhi, India, for providing research facilities. Shobhita Singal is thankful to CSIR for providing a senior research fellowship. We are also thankful to Bhaskar Gahtori, for technical help on SEM micrographs.

References

1 A. K. Geim, Graphene: Status and Prospects, *Science*, 2009, **324**, 1530.
2 M. Pumera, Voltammetry of Carbon Nanotubes and Graphenes: Excitement, Disappointment, and Reality, *Chem. Rec.*, 2012, **12**, 201.
3 A. A. Balandin, S. Ghosh, W. Bao, I. Calizo, D. Teweldebrhan, F. Miao and C. Lau Ning, Superior thermal conductivity of single-layer graphene, *Nano Lett.*, 2008, **8**, 902.
4 A. H. C. Neto, F. Guinea, N. M. R. Peres, K. S. Novoselov and A. K. Geim, The electronic properties of graphene, *Rev. Mod. Phys.*, 2009, **81**, 109.
5 D. A. C. Brownson and C. E. Banks, Graphene electrochemistry: an overview of potential applications, *Analyst*, 2010, **135**, 2768.
6 P. V. Kamat, Graphene-based nanoassemblies for energy conversion, *J. Phys. Chem. Lett.*, 2011, **2**, 242.
7 M. Pumera, Graphene-based nanomaterials and their electrochemistry, *Chem. Soc. Rev.*, 2010, **39**, 4146.
8 G. H. Moon, Y. Park, W. Kim and W. Choi, Photochemical loading of metal nanoparticles on reduced graphene oxide sheets using phosphotungstate, *Carbon*, 2011, **49**, 3454.
9 W. Yang, K. R. Ratinac, S. R. Ringer, P. Thordarson, J. J. Gooding and F. Braet, Carbon nanomaterials in biosensors: should you use nanotubes or graphene, *Angew. Chem., Int. Ed.*, 2010, **49**, 2114.
10 Z. H. Ni, H. M. Wang and J. Kasimet, Graphene thickness determination using reflection and contrast spectroscopy, *Nano Lett.*, 2007, **7**, 2758.
11 J. C. Meyer, A. K. Geim, M. I. Katsnelson, K. S. Novoselov, T. J. Booth and S. Roth, The structure of suspended graphene sheets, *Nature*, 2007, **446**, 60.
12 J. J. Gooding, A. Chou, J. Liu, D. Losic, J. G. Shapter and D. B. Hibbert, The effects of the lengths and orientations of singlewalled carbon nanotubes on the electrochemistry of nanotube modified electrodes, *Electrochem. Commun.*, 2007, **9**, 1677.
13 P. Avouris, Z. Chen and V. Perebeinos, Carbon-based electronics, *Nat. Nanotechnol.*, 2007, **2**, 605.
14 M. Pumera, Carbon nanotubes contain residual metal catalyst nanoparticles even after washing with nitric acid at elevated temperature because these metal nanoparticles are sheathed by several graphene sheets, *Langmuir*, 2007, **23**, 6453.
15 C. P. Jones, K. Jurkschat, A. Crossley, A. Compton, B. L. Riehl and C. E. Banks, Use of high-purity metal-catalyst-free

multiwalled carbon nanotubes to avoid potential experimental misinterpretations, *Langmuir*, 2007, **23**, 9501.
16 K. Gong, S. Chakrabarti and L. Dai, Electrochemistry at carbon nanotube electrodes: is the nanotube tip more active than the sidewall?, *Angew. Chem., Int. Ed.*, 2008, **47**, 5446.
17 D. Yu and L. Dai, Self-Assembled Graphene/Carbon Nanotube hybrid films for supercapacitors, *J. Phys. Chem. Lett.*, 2010, **1**, 467.
18 K. H. Yu, G. H. Lu, Z. Bo, S. Mao and J. H. Chen, Carbon nanotube with chemically-bonded graphene leaves for electronic and optoelectronic applications, *J. Phys. Chem. Lett.*, 2011, **2**, 1556.
19 D. Cai, M. Song and C. Xu, Highly conductive carbon-nanotube/graphite-oxide hybrid films, *Adv. Mater.*, 2008, **20**, 1706.
20 V. C. Tung, L. M. Chen, M. J. Allen, J. K. Wassei, K. Nelson and R. B. Kaner, Low-temperature solution processing of graphene–carbon nanotube hybrid materials for high-performance transparent conductors, *Nano Lett.*, 2009, **9**, 1949.
21 Y. Wang, Y. Wu, Y. Huang, F. Zhang, X. Yang and Y. Ma, Preventing graphene sheets from restacking for high capacitance performance, *J. Phys. Chem. C*, 2011, **115**, 23192.
22 S. B. Bon, L. Valentini, J. M. Kenny, L. Peponi, R. Verdejo and M. A. Lopez- Manchado, Electrodeposition of transparent and conducting graphene/carbon nanotube thin films, *Phys. Status Solidi A*, 2010, **207**, 2461.
23 H. R. Byon, S. W. Lee, S. Chen, P. T. Hammond and Y. Shao-Horn, Thin films of carbon nanotubes and chemically reduced graphene for electrochemical micro-capacitors, *Carbon*, 2011, **49**, 457.
24 Z. Fan, J. Yan, L. Zhi, Q. Zhang, T. Wei and J. Feng, A three dimensional carbon nanotube/graphene sandwich and its application as electrode in supercapacitors, *Adv. Mater.*, 2010, **22**, 3723.
25 S. Chen, P. Chen and Y. Wang, Carbon nanotubes grown *in situ* on graphene nanosheets as superior anodes for Li-ion batteries, *Nanoscale*, 2011, **3**, 4323.
26 P. Ammann, M. Pfisterer, T. Fehr and H. Rickli, Raised cardiac troponins: caused extend beyond acute coronary syndromes, *Br. Med. J.*, 2004, **328**, 1028.
27 S. Ko, B. Kim, S. S. Jo, S. Y. Oh and J. K. Park, Electrochemical detection of cardiac troponin I using a microchip with the surface-functionalized poly (dimethylsiloxane) channel, *Biosens. Bioelectron.*, 2007, **23**, 51.
28 V. Bhalla, S. Carrara, P. Sharma, Y. Nangia and C. R. Suri, Gold nanoparticles mediated label-free capacitance detection of cardiac troponin I, *Sens. Actuators, B*, 2012, **161**, 761.
29 A. Qureshi, Y. Gurbuz and J. H. Niazi, Biosensors for cardiac biomarkers detection: A review, *Sens. Actuators, B*, 2012, **171**, 62.
30 Rajesh, R. K. Paul and A. Mulchandani, Platinum nanoflowers decorated three-dimensional graphene-carbon nanotubes hybrid with enhanced electrocatalytic activity, *J. Power Sources*, 2013, **223**, 23.
31 A. Chou, T. Bocking, N. K. Singh and J. J. Gooding, Demonstration of the importance of oxygenated species at the end of carbon nanotubes on their favorable electrochemical properties, *Chem. Commun.*, 2005, **7**, 842.
32 Z. H. Ni, H. M. Fan, Y. P. Feng, Z. X. Shen, B. J. Yang and Y. H. Wu, Raman spectroscopic investigation of carbon nanowalls, *J. Chem. Phys.*, 2006, **124**, 204703.
33 C. Liu, H. Zhang, Y. Tang and S. Luo, Controllable growth of graphene/Cu composite and its nanoarchitecture-dependent electrocatalytic activity to hydrazine oxidation, *J. Mater. Chem. A*, 2014, **2**, 4580.
34 M. F. Smiechowski, V. F. Lvovich, S. Roy, A. Fleischman, W. H. Fissell and A. T. Riga, Electrochemical detection and characterization of proteins, *Biosens. Bioelectron.*, 2006, **22**, 670.
35 Y. Huang and I. I. Suni, Degenerate Si as an electrode material for electrochemical biosensors, *J. Electrochem. Soc.*, 2008, **155**, 350.
36 M. M. Billah, H. C. W. Hays, C. S. Hodges, S. Ponnambalam, R. Vohra and P. A. Millner, Mixed self-assembled monolayer (mSAM) based impedimetric immunosensors for cardiac troponin I (cTnI) and soluble lectin-like oxidized low-density lipoprotein receptor-1 (sLOX-1), *Sens. Actuators, B*, 2012, **173**, 361.
37 A. Periyakaruppan, R. P. Gandhiraman, M. Meyyappan and J. E. Koehne, Label free detection of cardiac troponin-I using carbon nanofiber based nanoelactrode array, *Anal. Chem.*, 2013, **85**, 3858.
38 A. A. Shumkov, E. V. Suprun, S. Z. Shatinina, A. V. Lisitsa, V. V. Shumyantseva and A. I. Archakov, Gold and silver nanoparticles for electrochemical detection of cardiac troponin I based on stripping voltammetry, *J. Bionanosci.*, 2013, **3**, 216.
39 T. O. Regan, M. Pravda, C. K. O. Sullivan and G. G. Guilbault, Development of biosensor array for rapid detection of cardiac markers: Immunosensor for detection of free cardiac troponin I, *Anal. Lett.*, 2003, **36**, 1903.
40 A. J. S. Ahammad, Y. H. Choi, K. Koh, J. H. Kim, J. J. Lee and M. Lee, Electrochemical detection of cardiac biomarker troponin I at gold nanoparticle-modified ITO electrode by using open circuit potential, *Int. J. Electrochem. Sci.*, 2011, **6**, 1906.